X-ray Emission from Comets

T. E. Cravens

The discovery of x-ray emission from comet Hyakutake was surprising given that comets are known to be cold. Observations by x-ray satellites such as the Röntgen Satellite (ROSAT) indicate that x-rays are produced by almost all comets. Theoretical and observational work has demonstrated that charge-exchange collisions of highly charged solar wind ions with cometary neutral species can explain this emission. X-ray observations of comets and other solar system objects may be used to determine the structure and dynamics of the solar wind.

Extreme ultraviolet (EUV) radiation, with wavelength (λ) ranging from ≈10 to 120 nm, and x-ray radiation, with λ between about 0.01 and 10 nm, are important for solar system and astrophysical applications because the photons are sufficiently energetic to ionize neutral atoms and molecules (*1*). X-ray emission in space is generally thought to originate from hot collisional plasmas, such as the 10^6 K gas found in the solar corona (*2*) or the 10^8 K gas observed in supernova remnants (*3*). The Sun is not the only source of x-rays in the solar system (*4*). X-rays are observed in the aurora at Earth and at Jupiter, and solar x-rays scattered off the surface of the Moon have been observed. Nonetheless, the 1996 discovery, using ROSAT (*5*), of strong x-ray emission from Hyakutake was surprising because cometary atmospheres are cold (*6*). The total x-ray power, or luminosity, of Hyakutake was measured to be about 10^9 W. EUV emission from Hyakutake was also seen by ROSAT (*5*) and by the Extreme Ultraviolet Explorer (EUVE) satellite (*5*). Hard x-rays with energies in excess of about 2 keV were not observed (*7*).

University of Kansas, Department of Physics and Astronomy, Malott Hall, Lawrence, KS 66045, USA. E-mail: cravens@ukans.edu

Shortly after the Hyakutake observations, soft x-ray emission from five other comets was also found, in the archived ROSAT observational database (*8*). EUV and soft x-ray emissions were then reported from several other comets (*9*), for a total of 14 comets. We now recognize that x-ray emission is a characteristic of all active comets.

Comets and Their X-ray Characteristics

A comet is a mixture of frozen H_2O, CO, CH_4, H_2CO, NH_3, and dust, with an ice-to-dust ratio of about unity, although it differs from comet to comet (*10–13*). When a comet (i.e., the nucleus, which is only a few km across) is far from the Sun, the mixture remains frozen, but the surface heats up, and volatiles are released (*11*) as the comet enters the inner solar system. The vapor produced by the now-active nucleus escapes into space, where it becomes the cometary coma, or atmosphere. The neutral gas coma extends far out into space (10^6 km), and the gas density varies inversely as the square of the cometocentric distance (*14*). The gas atoms and molecules can be photodissociated or photo ionized by solar radiation, creating additional neutral and ion species. The outflowing gas carries large quantities of dust along with it (*15*). What we see as a "visible" comet is mainly sunlight reflected from the extensive (≈10^5 km) dust coma and tail, created when solar radiation pressure pushes dust grains antisunward.

X-ray emission has been observed from 14 comets, and any physical mechanism that purports to explain this emission must account for four primary features of these observations: total luminosity, spatial morphology, temporal variation, and energy spectrum. The observed x-ray luminosity (L_x) of comet Hyakutake (*5*) was 4×10^8 W, for an aperture radius at the comet of 1.2×10^5 km (*16*). Observations of several comets have demonstrated that L_x correlates better with the gas production rate (Q) than it does with the dust production rate (*5*, *8*, *17–21*). All cometary EUV or x-ray images obtained so far (*5*, *8*, *17*), including recent images of comet C/LINEAR 1999 S4 from the Chandra X-ray Observatory (CXO) (*22*, *23*), exhibit similar spatial morphologies (Fig. 1). The x-ray brightness gradually decreases with increasing cometocentric distance (r), with a dependence of about r^{-1} or r^{-2} (*20*), merging with the background emission at distances of 10^5 to 10^6 km (*8*, *24*). The region of peak emission is crescent shaped with a brightness peak displaced toward the Sun. Cometary x-ray emissions also vary with time (*5*, *18*, *25*) and have been shown to correlate with the solar wind flux. Until a year or so ago, all published cometary x-ray spectra had very low spectral/energy resolution (*5*, *26*, *27*), and any continuum emission [such as that produced by the thermal bremsstrahlung (German for braking radiation) mech-

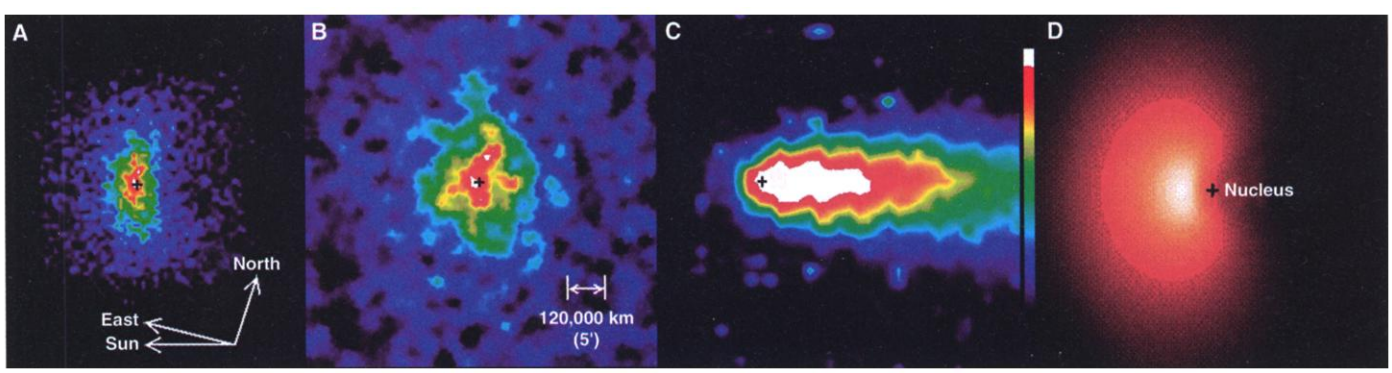

Fig. 1. (**A** to **C**), images of comet C/LINEAR 1999 S4 from July 2000 (*22*). (A) Chandra X-ray Observatory ACIS-S soft x-rays (energies 0.20 to 0.80 keV). (B) EUVE satellite EUV fluxes (energies 0.09 to 0.25 keV). (C) Visible light image, showing a coma and tail. (**D**) shows a simulated image of comet Hyakutake from an MHD model [adapted from (*49*)]. The Sun is toward the left in each case, the plus signs mark the position of the nucleus, and a spatial scale is shown for the observations. The scale for the simulation is approximately the same.

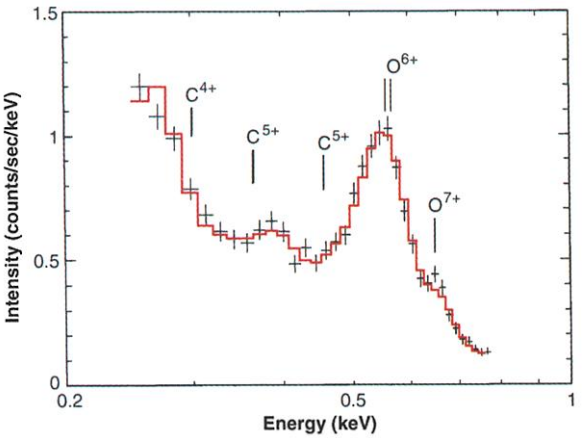

Fig. 2. Intensity versus photon energy. Soft x-ray spectrum of comet C/LINEAR 1999 S4 obtained on July 14, 2000, by the Chandra X-ray Observatory ACIS-S instrument. The solid red line is from a six-line best-fit "model" in which the line positions were fit parameters. The observational full-width half-maximum energy resolution was $\Delta E = .11$ keV. The positions of several transition lines from multiply charged ions known to be present in the solar wind are indicated but were not part of the data fit. Adapted from (*22*).

anism] could not be distinguished from a multiline spectrum. The CXO measured soft x-ray spectra from comet C/LINEAR 1999 S4 (*22*), with high enough resolution for several lines to be evident (Fig. 2). Spectra of Hyakutake from the EUVE satellite were also reported and show individual transition lines (*28*).

Comets and the Solar Wind

The solar wind plays a central role in several of the proposed x-ray production mechanisms. The solar wind originates in the 10^6 K solar corona and is a highly ionized but tenuous gas (i.e., a plasma) (*29*). The solar corona is collisionally ionized, but as it flows out into the solar system, it becomes increasingly dilute and collisions become infrequent. The corona is a powerful x-ray source. Active regions, which are associated with closed loops of magnetic field, are hotter [i.e., temperature (T) $\approx 2 \times 10^6$ K] and brighter in x-rays than are quiet regions ($T \approx 10^6$ K). The composition of both the solar wind and corona is "solar"—92% hydrogen, 8% helium, and 0.1% heavier elements, by volume. Heavier species are highly charged (e.g., have oxygen in the form of O^{7+} or O^{6+} ions, retaining only one or two orbital electrons) due to the high temperatures (*25*, *29*).

The solar wind makes a transition from subsonic to supersonic near the Sun (*30*, *31*), and the gas also cools as it expands such that by the time 1 astronomical unit (AU) is reached, the temperature has dropped down from $\approx 10^6$ K to a cool 10^5 K (*32*). However, the composition and charge-state distribution are frozen in at coronal values because of the rapidly decreasing collision frequency (*33*). The solar wind contains structure, such as slow (400 km/s) and fast (700 km/s) streams, most of which can be mapped back to the Sun. The solar wind eventually collides with the interstellar medium at a distance from the Sun of about 100 AU (*34*), although interaction with interstellar neutral species occurs closer to the Sun. A very small part of the solar wind encounters, and interacts with, the planets and comets.

The solar wind becomes contaminated with cometary ion species when cometary neutrals are ionized either by solar radiation or by the solar wind. The addition of mass slows down the solar wind (*35*), and a bow shock forms upwind of the comet (Fig. 3). The flow changes from supersonic to subsonic across this shock, located at $r \approx 4 \times 10^5$ km for comet Halley. Closer to the nucleus, inside a boundary called the cometopause, the cometary gas density is high, collisions are frequent, and the flow almost completely stagnates (*36*, *37*). The x-ray brightness peak resides within this boundary. Magnetic field lines pile up into a magnetic barrier in this stagnation region and drape around the head of the comet, forming in the downwind direction an observable (in visible light) magnetic/plasma tail, which is distinct from the dust tail (*38*).

Proposed X-ray Mechanisms

Possible mechanisms for cometary x-rays included thermal bremsstrahlung associated with collisions of solar wind electrons with cometary neutral gas or dust (*39*–*44*), microdust collisions (*45*), K-shell ionization of cometary neutrals by electron impact (*46*), scattering or fluorescence of solar x-rays by cometary gas or by small dust grains (*46*, *47*), and the solar wind charge exchange (SWCX) mechanism (*48*–*54*). In the thermal bremsstrahlung mechanism, fast electrons are deflected in collisions with charged targets, such as the nuclei of atoms, and emit continuum radiation (*46*). Electron energies in excess of 100 eV are needed (i.e., $T > 10^6$ K) for the production of x-ray photons. In the K-shell mechanism, a fast electron collision removes an orbital electron from an inner shell of the target atom. An early evaluation of these various mechanisms (*46*, *55*) favored just two of them: the SWCX mechanism (*48*) and the scattering of solar radiation from small [i.e., attogram (10^{-19} g)] dust grains.

A problem with mechanisms involving solar wind electrons (i.e., bremsstrahlung or K-shell ionization) is that the predicted luminosities are too small by factors of 100 to 1000, because the fluxes of high-energy electrons measured near comets are inadequate (*4*, *54*, *56*). Another difficulty is that x-ray emission has been observed out to great distances from the nucleus (10^5 to 10^6 km), beyond the bow shock, and the unshocked solar wind electrons at these distances are known to have energies of only about 10 eV. In addition, the observed spectra showing multiple emission lines have finally put to rest the idea that a continuum-type mechanism, or a mechanism producing only a couple of K-shell lines, can be the primary source of cometary x-rays.

Mechanisms based on dust grains also have run into a number of problems. When applied to ordinary cometary dust grains (i.e., about 1 μm in diameter), these mechanisms cannot produce the observed L_x. To overcome this difficulty, a population of attogram grains was invoked (*46*, *47*); however, the abundance of these grains is not known. X-ray emission is observed to vary with a comet's gas production rate and not with the dust production rate (*54*, *55*); furthermore, observed time variations of x-ray

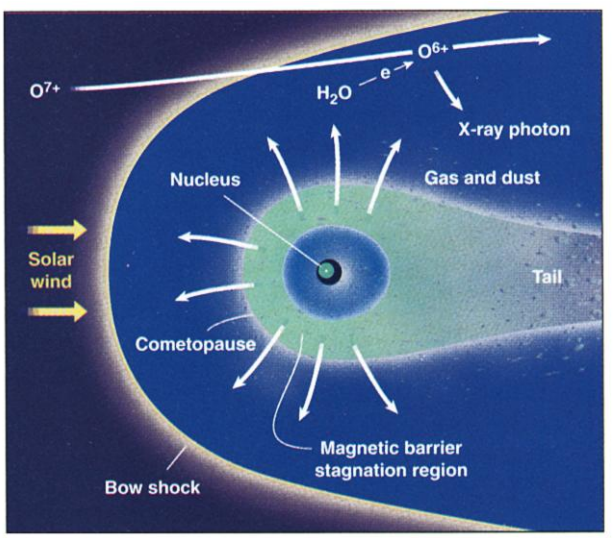

Fig. 3. Scheme of the solar wind/comet interaction. The location of the bow shock, magnetic barrier, and tail are shown. Also represented is a CT collision between a heavy solar wind ion and a cometary neutral water molecule, followed by the emission of an x-ray photon. The Sun is toward the left.

emission (*18*, *25*) correlate with the solar wind ion flux and not with solar x-ray intensity. Evidently, we can also exclude as a major x-ray source any dust-related mechanism. The only remaining viable mechanism that can account for a major part of cometary EUV and soft x-ray emission is the SWCX mechanism (*48*).

Minor ions in the solar wind exist in highly charged states (*29*, *52*), including species such as O^{7+}, O^{6+}, C^{6+}, C^{5+}, N^{6+}, Ne^{8+}, Si^{9+}, and Fe^{12+}. Experimental and theoretical work in atomic and molecular physics tells us that such ions readily undergo charge transfer reactions in which an incident ion removes an electron from a target neutral atom or molecule (*57*–*59*). The product ion remains highly charged and is almost always left in an excited state. This charge transfer (CT) reaction can be represented by:

$$A^{q+} + B \rightarrow A^{(q-1)+*} + B^{+}$$

where A denotes the projectile (e.g., O, C, Si, and so forth), q is the projectile charge (e.g., q = 5, 6, or 7) and B denotes the cometary target species (e.g., H_2O, OH, CO, O, H, and so forth). The excited (denoted by *) product ion de-excites by emitting one or more photons [$A^{(q-1)+*} \rightarrow A^{(q-1)+} + h\nu$, where $h\nu$ represents a photon]. For species and charge states relevant to comets, the principal quantum number of the ion $A^{(q-1)+*}$ is usually about n = 4, 5, or 6. The classical over-barrier model (*60*, *61*), although not as accurate as other atomic collision theories (*62*), graphically illustrates why the product ions are so highly excited (Fig. 4). The de-excitation usually takes place by cascading through intermediate states rather than by a single transition to the ground state. If q is large enough (e.g., q > 4 for oxygen), then at least some of the transitions lead to the emission of x-ray photons (*63*); otherwise, the transition energies are smaller, and non–x-ray photons are emitted.

An estimate of the local x-ray power density (P_x) can be obtained if only a single CT collision occurs during the course of a solar wind ion's journey through the comet. This collisionally thin approximation yields the expression $P_x = \alpha n_{sw} u_{sw} n_n$, where n_{sw}, u_{sw}, and n_n are the solar wind proton density, solar wind speed, and neutral target density, respectively (*48*). All the atomic and molecular details, as well as the solar wind heavy ion fraction f_h, are swept into the parameter α, which is given by $\alpha \approx f_h \langle\sigma_{ct}\rangle E_{ave}$, where $\langle\sigma_{ct}\rangle$ is an average CT cross section for all species and charge states and E_{ave} is an average photon energy. Integration of P_x over the volume containing cometary neutrals (or as defined by the observational aperture) yields L_x, which is thus proportional to Q, in agreement with the observations. With this model, time variations of the solar wind flux directly translate into time variations of the x-ray emission and thus satisfy observations of this correlation (*25*).

A more careful treatment of the SWCX mechanism is needed to model the spatial morphology and the spectrum. A complication is that multiple CT collisions take place in regions close to the nucleus, where the target density is high (i.e., the collisionally thick case). The charge state is reduced by 1 during each CT collision, such that for an extreme case an ion is converted into a neutral atom. When the charge state becomes too low, x-ray photons are no longer emitted. This effect explains the observed crescent-shaped emission with its sunward-displaced peak (Fig. 1). Numerical simulations of the solar wind interaction with Hyakutake including SWCX have been used to generate x-ray images. A global magnetohydrodynamic (MHD) model (*49*) and a hydrodynamic model (*50*) were used to predict solar wind speeds and densities and the x-ray emission around a comet. The simulated x-ray images are remarkably similar to the observed images (Fig. 1).

The theoretical energy spectra obtained using SWCX are in good agreement with low-resolution measurements, but the careful comparisons and calculations needed to interpret the newer high-resolution observations, which show specific emission lines, have not yet been undertaken. Some theories included only a few solar wind species but used a careful cascading scheme (*51*), whereas others used a simple cascading scheme and simple classical overbarrier collision cross sections but included a larger number of solar wind ions and charge states (*50*, *52*). One complication is that spectral differences are expected for slow and fast solar wind streams, with the slow solar wind, with its higher coronal freeze-in temperature, producing a harder (i.e., more energetic photons) spectrum than does the fast solar wind (*52*). Kharchenko and Dalgarno (*51*, *53*) treated the cascading process accurately but worked with a simple solar wind interaction model. They predicted the existence of a large number of emission lines of highly charged ions, including the following: O^{5+} ($1s^2 5d \rightarrow 1s^2 2p$) at 106.5 eV, C^{4+} ($1s2s \rightarrow 1s^2$) at 298.9 eV, C^{5+} ($2p \rightarrow 1s$) at 367.3 eV, C^{5+} ($4p \rightarrow 1s$) at 459.2 eV, O^{6+} ($1s2p \rightarrow 1s^2$) at 568.4 eV, and O^{6+} ($1s2s \rightarrow 1s^2$) at 560.9 eV. At least some of these lines appear in the CXO spectrum of comet C/LINEAR 1999 S4. For example, most of the CXO peak measured near .56 keV (*22*) is certainly a combination of the two O^{6+} lines just mentioned (which comes from CT of solar wind O^{7+}), and the CXO line located at .32 keV may be due to C^{4+} ($1s2s \rightarrow 1s^2$). Similar identifications can be made in the EUVE spectrum of comet Hyakutake (*28*).

The SWCX mechanism successfully explains the observations. Further theoretical progress will require the integration of several ingredients into a single model: (i) a suitable MHD model of the solar wind interaction, (ii) accurate solar wind composition for a range of solar wind types, and (iii) a more complete set of state-specific CT cross sections for cometary target species from laboratory measurements and atomic theory. Most past measurements were not carried out for cometary target species such as H_2O, or for collision energies relevant to the solar wind, or with sufficiently detailed information on the ion final states. However, recent experimental work has started to address these issues, motivated in part by the cometary x-ray problem (*62*, *64*–*69*). For ex-

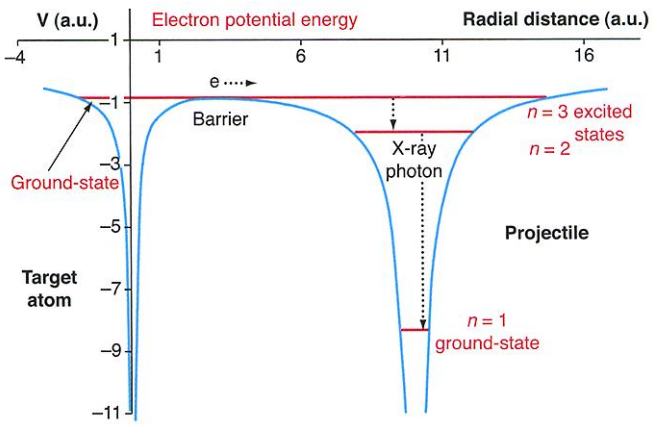

Fig. 4. Electron potential energy V [in atomic units (a.u.)] versus distance from the target atom nucleus (assumed to be atomic hydrogen here) for a charge transfer reaction involving projectile ion A^{q+} (calculated here for Be^{4+}). The internuclear distance chosen here [10 a.u. (1 a.u. = 1 Bohr radius = 5.29×10^{-11} m)] is the curve-crossing distance for the n = 3 ion final state. 1 atomic energy unit = 1 hartree = 27.2 eV. The target energy level (and binding energy) and product ion (Be^{3+}) energy levels are shown. In the classical overbarrier model, the electron is able to cross over from the target to the projectile for the favored principal quantum number ($n \approx 3$, here). A possible cascading pathway for the de-excitation by photon emission is shown.

ample, recent work indicates that multiple as well as single-electron CT makes a contribution to the x-ray emission (*62*, *69*).

Other Solar System X-ray Sources

The initially puzzling discovery that comets are x-ray sources can now be explained by the charge exchange of highly charged solar wind ions with neutral atoms and molecules that reside in the cometary atmosphere. The energy required to power this emission originates in the hot solar corona and is temporarily stored as potential energy in highly stripped solar wind ions until this energy is released by charge transfer collisions. X-ray or EUV observations of comets are, in effect, remotely sensing the solar wind; however, extraction of useful information on solar wind properties from such observations will require further improvement in our understanding of the SWCX mechanism. The SWCX mechanism operates wherever the solar wind (or any highly ionized plasma) interacts with neutral gas (*4*, *55*) and has also been suggested as a source of x-ray emission from Venus and Mars (*4*, *70–72*), the terrestrial hydrogen geocorona (*55*, *73–76*), and interstellar neutral gas (*4*, *73*, *74*, *76–78*).

References and Notes

1. A photon is a unit, or quantum, of electromagnetic radiation and has energy (E) = hc/λ, where h is Planck's constant and c is the speed of light. For example, an x-ray photon with λ = 1 nm has an E = 1240 eV, where 1 eV = 1.602×10^{-19} J is an energy unit. X-ray photons have energies greater than about 100 eV.
2. P. Foukal, *Solar Astrophysics* (Wiley, New York, 1990).
3. D. F. Cioffi, in *Physical Processes in Hot Cosmic Plasma*, W. Brinkmann, A. C. Fabian, F. Giovannelli, Eds. (Kluwer, Dordrecht, Netherlands, 1990), pp. 1–16.
4. T. E. Cravens, *Adv. Space Res.* **26**, 1443 (2000).
5. One earlier x-ray observation of comet C/1979 Y1 (Bradfield) by the orbiting Einstein observatory yielded negative results (*7*). Lisse *et al.* reported on measurements made with two ROSAT instruments and one Rossi X-ray Timing Explorer (XTE) instrument. These instruments were the high-resolution imager (HRI), with a spectral range (or band pass) of 0.10 to 2.0 keV (i.e., soft x-rays); the wide-field camera, with a spectral range in the S1A filter used of 0.09 to 0.206 keV (i.e., EUV emission); and the XTE proportional counter array (PCA), with a spectral range of 2 to 60 keV. The XTE PCA observations were negative (*79*). EUV emission was also observed by the EUVE satellite (*17*).
6. For a thorough treatment of cometary physics, consult R. I. Newburn Jr., M. Neugebauer, J. Rahe, Eds., *Comets in the Post-Halley Era* (Kluwer, Dordrecht, Netherlands, 1991).
7. H. S. Hudson, W.-H. Ip, A. Mendis, *Planet. Space Sci.* **29**, 1373, (1981).
8. Four of the comets were observed in 1990 and 1991 with the ROSAT position-sensitive proportional counter (PSPC), and a fifth new comet was observed in 1996 with the HRI (comet C/1996 Q1 Tabur). The four comets are C/1990 K1 (Levy), C/1990 N1 (Tsuchiya-Kiuchi), 45P (Honda-Mrkos-Pajdusakova), and C/1991 A2 (Arai). The ROSAT all-sky survey was carried out with the PSPC, which had a spectral range of 0.1 to 2.4 keV, but had a spectral resolution of about $\Delta E/E$ = 0.5 to 1 in the energy range of interest, where E is the photon energy and ΔE is the energy resolution (*80*).
9. Emission was observed from comets Encke (*18*, *19*), Hale-Bopp (C/1995 Q1) (*17*, *19–21*), Bradfield (C/1995 Q1) (*17*), 6P/d'Arrest (*17*), Mueller (C/1993 A1) (*19*), 19P/Borrelly (*19*), and C/LINEAR 1999 S4 (*22*).
10. F. L. Whipple, *Astrophys. J.* **111**, 375 (1950).
11. A. H. Delsemme, in (*6*), pp. 377–428.
12. D. Krankowsky *et al.*, *Nature* **321**, 326 (1986).
13. Z. Sekanina, in (*6*), pp. 769–824.
14. A simple spherically symmetric approximation to the neutral density in the cometary coma as a function of cometocentric distance r is given by $n_n = Q/[4\pi u_n r^2]$, for r less than the ionization scale length $R = u_n\tau$, where $\tau \approx 10^6$ s (for 1 AU) is the ionization lifetime, and $u_n \approx 1$ km/s is the neutral gas outflow speed.
15. T. I. Gombosi, in (*6*), pp. 991–1004.
16. The luminosity depends on the energy bandpass and on the observational aperture at the comet. The luminosity for Hyakutake in photons/s for ROSAT and in soft x-rays (0.1 to 2 keV) was $Q_X \approx 10^{25}$ s^{-1}, whereas $Q_{EUV} \approx 7.5 \times 10^{25}$ s^{-1} for the EUVE satellite (.07 to .18 keV), both with an aperture radius from the comet of 120,000 km. Additional energy information is needed to obtain a power, or "energy" luminosity L_x.
17. M. J. Mumma, V. A. Krasnopolsky, M. J. Abbott, *Astrophys. J.* **491**, L125 (1997).
18. C. M. Lisse *et al.*, *Icarus* **141**, 2316, (1999).
19. V. A. Krasnopolsky, M. J. Mumma, M. J. Abbott, *Icarus* **146**, 152 (2000).
20. V. A. Krasnopolsky *et al.*, *Science* **277**, 1488, (1997).
21. C. M. Lisse *et al.*, *Earth Moon Planets* **77**, 283 (1999).
22. C. M. Lisse *et al.*, *Science* **292**, 1343 (2001).
23. Up-to-date information of x-ray observations by CXO of comets and other objects can be found at http://chandra.harvard.edu.
24. D. McCammon, W. T. Sanders, *Ann. Rev. Astron. Astrophys.* **28**, 657 (1990).
25. M. Neugebauer *et al.*, *J. Geophys. Res.* **105**, 20,949 (2000).
26. A. Owens *et al.*, *Astrophys. J.* **493**, L47 (1998).
27. The comet Levy spectrum in (*80*) was measured by the ROSAT PSPC with a $\Delta E/E$ of roughly 0.8 near 300 eV. The PSPC was not working for the 1996 Hyakutake observations reported by (*5*).
28. V. A. Krasnopolsky, M. J. Mumma, *Astrophys. J.* **549**, 629 (2001).
29. S. J. Bame, in *Solar Wind*, C. P. Sonnett *et al.*, Eds. (SP-308, NASA, 1972), pp. 535–558.
30. T. E. Cravens, *Physics of Solar System Plasmas* (Cambridge Univ. Press, Cambridge, 1997).
31. E. N. Parker, *Interplanetary Dynamical Processes* (Interscience/Wiley, New York, 1963).
32. The average properties of the solar wind at 1 AU are: proton number density ≈ 7 cm^{-3}, speed ≈ 450 km/s, temperature ≈ 10^5 K, magnetic field strength ≈ 5 nT, and Mach number ≈ 8.
33. A. J. Hundhausen, H. E. Gilbert, S. J. Bame, *J. Geophys. Res.* **73**, 5485 (1968).
34. S. T. Suess, *Rev. Geophys.* **28**, 97 (1990).
35. A. A. Galeev, in (*6*), pp. 1145–1170.
36. T. E. Cravens, in (*6*), pp. 1211–1258.
37. K. R. Flammer, in (*6*), pp. 1125–1144.
38. J. C. Brandt, in *Comets*, L. L. Wilkening, Ed. (Univ. Arizona Press, Tucson, 1982), pp. 519–537.
39. R. Bingham, J. M. Dawson, V. D. Shapiro, D. A. Mendis, B. J. Kellet, *Science* **275**, 49 (1997).
40. J. M. Dawson, R. Bingham, V. D. Shapiro, *Plasma Phys. Control. Fusion* **39**, A185 (1997).
41. T. G. Northrop, *Icarus* **128**, 480 (1997).
42. ———, C. M. Lisse, M. J. Mumma, M. D. Desch, *Icarus* **127**, 246 (1997).
43. M. Uchida, M. Morikawa, H. Kubotani, H. Mouri *Astrophys. J.* **498**, 863 (1998).
44. V. D. Shapiro, *J. Geophys. Res.* **104**, 2537 (1999).
45. W.-H. Ip, V. W. Chow, *Icarus* **130**, 217 (1997).
46. V. A. Krasnopolsky, *Icarus* **128**, 368 (1997).
47. N. C. Wickramasinghe, F. Hoyle, *Astrophys. Space Sci.* **239**, 121 (1996).
48. T. E. Cravens, *Geophys. Res. Lett* **25**, 105 (1997).
49. R. Häberli, T. I. Gombosi, D. L. DeZeeuw, M. R. Combi, K. G. Powell, *Science* **276**, 939 (1997).
50. R. Wegmann, H. U. Schmidt, C. M. Lisse, K. Dennerl, J. Englhauser, *Planet. Space Sci.* **46**, 603 (1998).
51. V. Kharchenko, A. Dalgarno, *J. Geophys. Res.* **105**, 18,351 (2000).
52. N. A. Schwadron, T. E. Cravens, *Astrophys. J.* **544**, 558 (2000).
53. V. Kharchenko, A. Dalgarno, *Astrophys. J.* **554**, L99, 2001.
54. V. Krasnopolsky, in press.
55. K. Dennerl, in *Atomic Physics 16*, W. E. Baylis, G. W. F. Drake, Eds. (American Institute of Physics, New York, 1999), pp. 361–376.
56. Giotto measured lower electron fluxes than the VEGA spacecraft for $E > 100$ eV in the inner coma of comet Halley (*54*, *81*). The Giotto fluxes would give lower x-ray intensities, but in either case the x-ray emission is too small.
57. R. A. Phaneuf, I. Alvarez, F. W. Meyer, D. H. Crandall, *Phys. Rev. A* **26**, 1892 (1982).
58. D. Dijkamp, *J. Phys. B* **18**, 737 (1985).
59. H. B. Gilbody, *Adv. At. Mol. Opt. Phys.* **22**, 143 (1986).
60. H. Ryufuku, K. Sasabi, T. Watanabe, *Phys. Rev. A* **21**, 745 (1980).
61. R. Mann, F. Folkmann, H. F. Beyer, *J. Phys. B* **14**, 1161 (1981).
62. A. A. Hasan, F. Eiassa, R. Ali, D. R. Schultz, P. C. Stancil, *Astrophys. J.* **560**, L201 (2001).
63. Species having a single orbital electron and nuclear charge Z have hydrogen-like energy levels (iso-hydrogenic) and transition energies. Relevant species include O^{7+}, N^{6+}, and C^{5+}. The energy of a state with principal quantum number n is given by: $E_n = -Z^2 13.6\text{eV}/n^2$.
64. J. B. Greenwood, I. B. Williams, S. J. Smith, A. Chutjian, *Astrophys. J.* **533**, L175 (2000).
65. ———, *Phys. Rev. A* **63**, 62707 (2001).
66. P. Beiersdorfer *et al.*, *Phys. Rev. Lett.* **85**, 5090 (2000).
67. P. Beiersdorfer, C. M. Lisse, R. E. Olson, G. V. Brown, H. Chen, *Astrophys. J.* **549**, L147 (2001).
68. A. Chutjian, in press.
69. J. B. Greenwood's Web site provides an excellent and up-to-date review of laboratory studies relevant to SWCX and can be found at www.qub.ac.uk/mp/ampr/networks/cometxrays.htm.
70. M. Holmström, S. Barabash, E. Kallio, *Geophys. Res. Lett.* **28**, 1287 (2001).
71. V. Krasnopolsky, *Icarus* **148**, 597 (2000).
72. T. E. Cravens, A. N. Maurellis, *Geophys. Res. Lett.* **28**, 3043 (2001).
73. D. P. Cox, in *The Local Bubble and Beyond*, D. Breitschwerdt, M. J. Freyberg, J. Trümper, Eds. (Springer, Berlin, 1998), pp. 121–132.
74. T. E. Cravens, *Astrophys. J.* **532**, L153 (2000).
75. M. J. Freyberg, in *The Local Bubble and Beyond*, D. Breitschwerdt, M. J. Freyberg, J. Trümper, Eds. (Springer, Berlin, 1998), pp. 113–116.
76. T. E. Cravens, I. P. Robertson, S. L. Snowden, *J. Geophys. Res.* **106**, 24883 (2001).
77. I. P. Robertson, T. E. Cravens, S. L. Snowden, T. Linde, *Space Sci. Rev.* **97**, 401 (2001).
78. B. J. Wargelin, J. J. Drake, *Astrophys. J.* **546**, L57 (2001).
79. C. M. Lisse *et al.*, *Science* **274**, 205 (1996).
80. K. Dennerl, J. Englhauser, J. Trümper, *Science* **277**, 1625 (1997).
81. T. E. Cravens, J. U. Kozyra, A. F. Nagy, T. I. Gombosi, M. Kurtz, *J. Geophys. Res.* **92**, 7341 (1987).

82. We thank V. Kharchenko, C. M. Lisse, K. Dennerl, and the referees for helpful comments. Supported by NASA Planetary Atmospheres grant NAG5-11038 and NSF grant ATM-9815574.